Optics & Laser Technology 141 (2021) 107145

Contents lists available at ScienceDirect

Optics and Laser Technology

journal homepage: www.elsevier.com/locate/optlastec

Full length article

High-power operation and lateral divergence angle reduction of broad-area laser diodes at 976 nm

Yuxian Liu [a,b], Guowen Yang [a,b,c,*], Zhenfu Wang [a], Te Li [a], Song Tang [c], Yuliang Zhao [a,b], Yu Lan [a,b], Abdullah Demir [d,*]

[a] State Key Laboratory of Transient Optics and Photonics, Xi'an Institute of Optics and Precision Mechanics, Chinese Academy of Sciences, Xi'an 710119, China
[b] University of Chinese Academy of Sciences, Beijing 100049, China
[c] Dogain Laser Technology (Suzhou) Co., Ltd., Suzhou 215123, China
[d] Bilkent University, UNAM - Institute of Materials Science and Nanotechnology, Ankara 06800, Turkey

ARTICLE INFO

Keywords:
Semiconductor laser
Diode laser
High power
High efficiency
Low divergence angle
High brightness
976 nm

ABSTRACT

Broad-area diode lasers with high output power and low lateral divergence angle are highly desired for extensive scientific and industrial applications. Here, we report on the epitaxial design for higher output power and a flared waveguide design for reduced divergence, which leads to high power operation with a low lateral divergence angle. A vertically asymmetric epitaxial structure was employed and optimized for low internal optical loss and high efficiency to realize high output power operation. Using a flared waveguide design, the lateral divergence angle was efficiently reduced by decreasing the number of high-order lateral optical modes significantly. The flared waveguide design introduces a smooth modification of the ridge width along the cavity without deteriorating laser performance. Based on the optimized epitaxial and waveguide design, we scaled the waveguide width to realize high continuous-wave power of 34.5 W at 25 °C. A low lateral divergence angle of 8° and high power conversion efficiency of 60% were achieved at the operating power level of 25 W. The life test data (30 A at 45 °C for 39 units, 0 failures in 1000 h) demonstrated reliable operation illustrating the efficient design for reduced lateral divergence angle and high operating power.

1. Introduction

The deployment of high-power laser diodes (LDs) ramped up enormously in the past two decades to meet the needs of various industrial applications [1]. Particularly, fiber laser (FL) and direct-diode systems are becoming powerful tools for material processing in the industry [2,3]. A high-performance laser system with an output power of 1–10 kW needs a large quantity (100–1000) of pump LDs. This places a stringent requirement for performance, quality, and reliability for the LD chips [3,4]. LDs at 915 nm and 976 nm are the most important pump sources for Yb-doped fiber lasers [5,6]. Especially, 976 nm LD has advantages as a pump source since its absorption peak is 3 times higher and a quantum defect is 5% lower than that of 915 nm LD. Hence, 976 nm LDs can greatly reduce the gain fiber length and improve the efficiency of the whole system, saving energy and cost. However, the performance of these FLs is still limited by the power, efficiency, and brightness of the 976 nm pump LDs. It is evident that improving the operating output power [7–10] and lateral divergence angle (i.e. beam quality) [11–14] of individual LDs would directly improve the performance and decrease the cost of these systems.

Progress in epitaxial growth technologies and the introduction of innovative or optimized epitaxial structures demonstrated a continuous increase in the output power of GaAs-based semiconductor lasers [7,8,9,10,15]. Detailed studies have been carried out to investigate the causes of laser power limitations. The laser output power is considered to be limited by various mechanisms such as linear losses (e.g. free-carrier absorption [16] and longitudinal spatial hole burning [9,10,17,18]), non-linear losses (e.g. two-photon absorption) [10,19], carrier leakage [16] and carrier non-pinning due to self-heating of the laser [20]. By employing novel designs to mitigate these effects, maximum continuous-wave (CW) power of 33 W [10] and pulse power of 145 W [21] at 25 °C have been realized for 100 μm wide broad-area waveguide lasers based on GaAs. At 976 nm, high single emitter CW power at 25 °C was reported by IPG photonics as 31 W [22] and Fujikura/Optoenergy as 33 W [23].

Another challenging problem limiting the LD performance is the lateral beam quality, which is inversely proportional to the lateral divergence angle (e.g. far-field angle containing 90% of the power,

* Corresponding authors.

https://doi.org/10.1016/j.optlastec.2021.107145
Received 6 December 2020; Received in revised form 30 March 2021; Accepted 12 April 2021
Available online 28 April 2021

$\theta_{90\%}$). Although the vertical cavity of LDs can be set as a single-mode by epitaxial design, the wide lateral size of the broad-area lasers (e.g. 20–250 μm) supports many lateral optical modes. Lateral divergence angle is an important figure of merit for an LD since its lower values lead to both higher brightness and better coupling into optical fibers. Understanding the contributing factors of beam quality has been the subject of intense research [24–26]. Various physical mechanisms (e.g. built-in index guiding, self-heating induced thermal lensing and carrier accumulation effects, lateral spatial hole burning) have been considered to influence the formation of lateral modes. These effects interact strongly with each other and their strength changes with the injected current. All these factors make it a complex phenomenon but typically result in a widening of lateral divergence angle (i.e. lateral far-field blooming) with the current increase for both pulsed (non-thermal effects [25]) and CW (strong thermal contribution [26]) operating LDs. A variety of structures has been developed to reduce the lateral divergence angle such as thermal lensing compensation [14], loss tailoring with microstructures for higher-order mode filtering [11,27,28], tapered laser structures consisting of a straight ridge waveguide and a tapered section for spatial mode filtering and light amplification [29–31], photonic crystal (PhC) for selectively deflecting the higher-order modes [32], periodic modulation of the pump with microscale patterned electrodes [33], and tailored phase structures [34]. All these methods showed beam quality improvement of LDs. However, they are usually demonstrated at low laser power levels suffering from output power degradation due to unintended losses, which limits their applicability. Realizing low lateral far-field divergence angle with high-power operation has a significant value for both research and industrial purposes.

In this paper, we employed an epitaxial structure with an efficient high-power operation and introduced a flared waveguide design for reduced divergence angle without sacrificing output power and efficiency. We developed an asymmetric broad waveguide epitaxial structure for low internal loss, a suitable optical confinement factor, and a low resistance by optimizing thickness and doping profiles to realize high power and efficiency. We demonstrated a multi-mode flared laser design by narrowing the waveguide width down slowly towards the high reflectivity coated back facet, which intended to limit the number of lateral higher-order modes and thus reduced lateral divergence angle. To evaluate the mechanism and effectiveness of the flared waveguide approach for mode filtering, we simulated the optical mode behavior for a 100 μm wide waveguide illustrating high-order mode suppression resulting in a lower lateral divergence angle. It is shown experimentally that such a waveguide provides a reduction of lateral divergence angle even at high power without sacrificing efficiency and threshold current. Then, we applied this design concept to LDs with a much wider waveguide and realized a record-high operating power with a low divergence angle. The life test results confirm the reliable operation of the epitaxial structure and waveguide design of these LDs.

2. Epitaxial chip design and device characterization for efficient laser operation

For the above-threshold operating region, the optical output power P_{out} of a LD can be expressed as:

$$P_{out} = \eta_s(I - I_{th}) = \eta_i \frac{\alpha_m}{\alpha_i + \alpha_m} \frac{hv}{q}(I - I_{th}) \quad (1)$$

where η_s is the slope, η_i is the internal quantum efficiency, α_m is the mirror loss, $\alpha_i$is the internal loss,I_{th} is the threshold current, hv is the photon energy, q is the electron charge [35]. The output power of LDs also depends on the operating temperature because of the temperature dependence of threshold current and slope [15], which can be defined by:

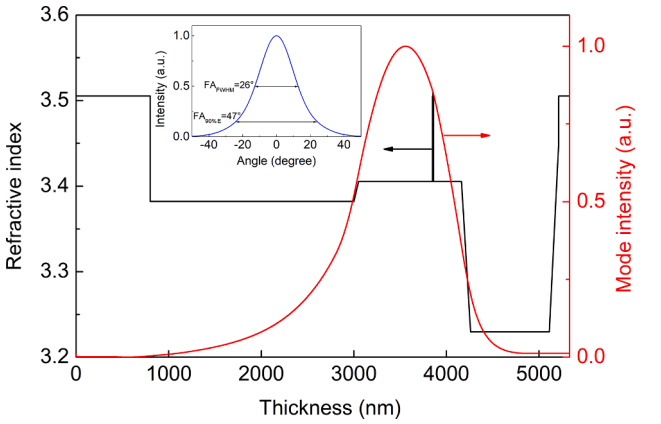

Fig. 1. Refractive index profile of the epitaxial structure and the simulation result of the vertical near-field profile. The inset shows the simulation result of the vertical far-field.

$$\eta_s(T) = \eta_s(T_r)\exp(-\frac{T - T_r}{T_1}) \quad (2)$$

$$I_{th}(T) = I_{th}(T_r)\exp(\frac{T - T_r}{T_0}) \quad (3)$$

whereT_r is the room temperature.T_0 and T_1 are the characteristic temperatures for the threshold current and slope efficiency, respectively, which characterizes the temperature sensitivity of the design.

To achieve high CW output power at high injection current, high slope and low temperature sensitivity of a design are key performance indicators. Then the following parameters play a significant role: (a) high internal quantum efficiency, η_i; (b) low internal optical absorption loss, α_i; (c) high characteristic temperatures, T_0 and T_1; (d) suitable optical confinement factor of the quantum well (QW) active region,Γ_{QW}.

The internal optical absorption loss can be approximated as the sum of the absorption loss of each layer j in the vertical structure expressed as [35,36]:

$$\alpha_i = \sum_j \Gamma_j(\sigma_n n_j + \sigma_p p_j) \quad (4)$$

where Γ_j is the optical confinement factor; n_j and p_j are the electron and hole carrier concentrations, respectively.σ_n and $\sigma_p$are the free carrier absorption coefficients for electrons and holes, respectively. The absorption coefficients are assumed to be equal to the cross-sections in the GaAs bulk material as$\sigma_n = 4 \times 10^{-18}$ cm^2 and$\sigma_p = 12 \times 10^{-18}$ cm^2, respectively [15]. Higher internal loss directly reduces the slope efficiency (Eq. (1)) and enhances the effect of longitudinal spatial hole burning (LSHB), which further reduces the output power [10]. Hence low internal absorption loss values are required to realize high power LDs.

Although the Eqs. (1)–(4) describe the basic P-I behavior through optical and active region parameters, the electrical characteristic of the chip needs to be involved to define the P-I-V model of a laser diode and optimize its efficiency. Here, the power conversion efficiency (PCE),η_c, can be empirically expressed as:

$$\eta_c = \frac{P_{out}}{P_{input}} = \frac{P_{out}}{I^2R_s + IV_0} \quad (5)$$

whereR_s is the series resistance and V_0 is the turn-on voltage. LowR_s and V_0 need to be addressed by epitaxial design. Higher PCE leading to lower waste heat is critical to realize very high CW output powers.

An asymmetric waveguide and cladding structure were developed by optimizing the thickness, doping level, and composition for each layer to obtain a balance of the optical confinement factor, optical loss, and

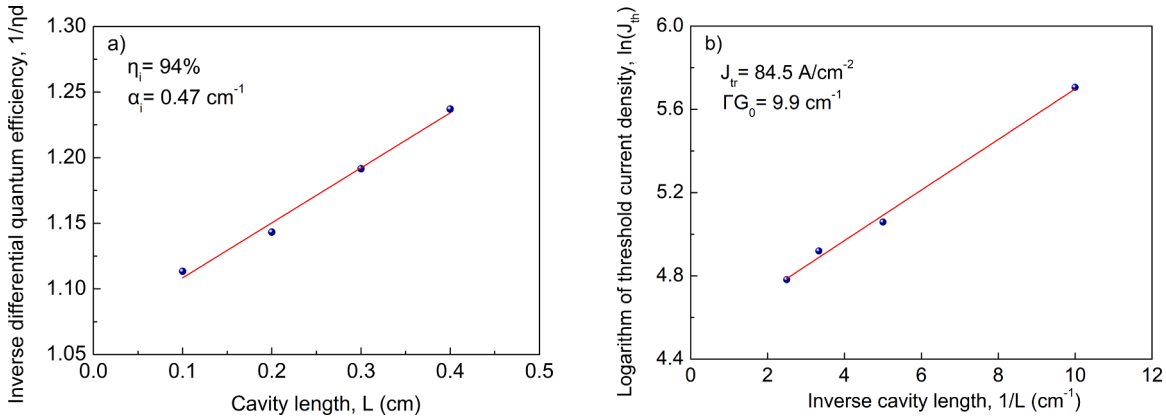

Fig. 2. Experimental results under pulsed operation for (a) the inverse differential quantum efficiency versus cavity length, and (b) the natural logarithm of threshold current density versus inverse cavity length.

Table 1
Simulated and measured internal performance parameters.

Characteristic parameters	Value
Simulated optical confinement factor,Γ	0.67%
Simulated (measured) internal optical loss, α_i	0.49 cm^{-1} (0.47 cm^{-1})
Simulated (measured) vertical far filed, $FA_{90\%E}$	47° (48.2°)
Measured internal quantum efficiency, η_i	94%
Measured transparency current density, J_{tr}	84.5 A/cm^2
Measured modal gain coefficient, ΓG_0	9.9 cm^{-1}

resistance. A thin p-waveguide was used to obtain a low resistance, low internal optical loss, and low bias-driven leakage currents. In contrast, a thick n-waveguide, and n-cladding are designed to have most of the optical mode in the n-side and realize low absorption loss as a result of the low free carrier absorption losses of the electrons. A modest optical confinement factor is employed to suppress COMD at a high current. At the same time, a suitable quantum well barrier height was introduced to improve the internal quantum efficiency and temperature stability by reducing the carrier leakage from the active region. The calculated profile of the refractive index and the intensity of the fundamental mode are shown in Fig. 1. The optical absorption loss of the structure is 0.49 cm^{-1} and the optical confinement factor of the active layer is 0.67% based on the simulation results. The calculated vertical far-field angle containing 90% of the intensity is 47° as shown in Fig. 1 (inset).

Based on the epitaxial design, growth and device fabrication were followed by the characterization of the internal parameters. Uncoated bare devices with 100 μm stripe width and four different cavity lengths were measured under pulsed operation with a low duty cycle (pulse width 100 μs, repetition rate 100 Hz) to extract the internal parameters of the epitaxial structure. The dependencies of the inverse differential quantum efficiency ($1/\eta_d$) on the cavity length (L) and the logarithm of the threshold current density ($\ln J_{th}$) on the inverse cavity length (1/L) are shown in Fig. 2(a) and 2(b), where each point represents the average data of five chips. By linear fitting of the results, the internal efficiency η_i, internal optical losses α_i, transparency current density J_{tr}, and modal gain coefficient ΓG_0 can be determined according to the equations [37]:

$$\frac{1}{\eta_d} = \frac{1}{\eta_i}\left(1 + \frac{2\alpha_i L}{\ln(\frac{1}{R_1 R_2})}\right) \tag{6}$$

$$\ln J_{th} = \ln J_{tr} + \left[\frac{1}{\Gamma G_0}(\alpha_i + \frac{1}{2L}\ln\frac{1}{R_1 R_2})\right] \tag{7}$$

Assuming a common facet reflectivity of $R_1 = R_2 = 0.3$ for the uncoated cavities, the internal quantum efficiency, internal optical loss, transparency current density, and modal gain coefficient are determined to be 94%, 0.47 cm^{-1}, 84.5 A/cm^2, and 9.9 cm^{-1}, respectively, as summarized in Table 1, including other key parameters of both simulation and measurement. The experimental value of the 0.47 cm^{-1} for the internal optical loss agrees well with the simulation result of 0.49 cm^{-1}. The low transparency current proves the high material quality and carrier confinement of the QW. The relatively low modal gain with the calculated confinement factor of 0.67% gives a G_0 value of 1478 cm^{-1}.

3. Flared waveguide design for efficiently reduced lateral divergence angle

Our approach is based on a multi-mode flared waveguide design with gentle modification of the ridge width for a broad area waveguide. A simplified design of the waveguide is illustrated in Fig. 3. The flared waveguide design consists of a single waveguide with a slight taper angle. A gain- or index-guided structure can realize the waveguide. The front facet reflectivity is anti-reflection (R_F = 1%), and the back facet is

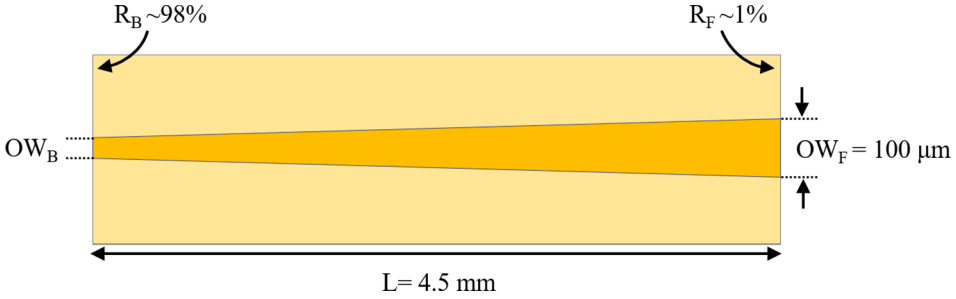

Fig. 3. Simplified illustration of the flared waveguide design with a narrow back open window width (OW_B < 100 μm) and wide front open window width (OW_F = 100 μm).

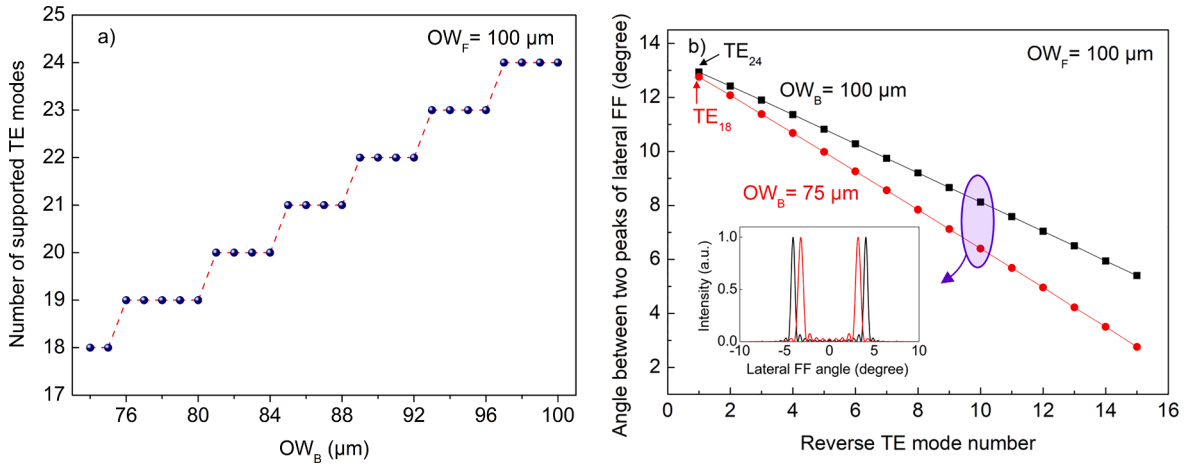

Fig. 4. Simulation results with OW_F of 100 μm for (a) the number of TE modes versus OW_B, and (b) the angle between two peaks of lateral FF versus reverse TE mode number for OW_B of 100 and 75 μm. The inset shows the lateral FF angle profile for the same reverse mode number.

high-reflection coated ($R_B > 95\%$). The laser waveguide width is narrowed down slowly towards the high reflectivity coated back facet, where a typical flare angle is between 0.1 and 0.4°. Since the number of lateral modes is proportional to the waveguide's width, the narrower back waveguide will support less guided optical modes, and thus suppressing higher order modes generated on the broader front waveguide. This mode filtering effect reduces the total number of optical modes in the laser cavity. Since the divergence angle is larger for a higher-order mode, a reduced number of modes result in a smaller lateral divergence angle. One common principle for the flared laser studied here and a typical tapered laser [29,30,31] is implementing the mode filtering effect. However, the geometry, mode content, and target power levels are dramatically different. A typical tapered laser consists of a narrow (e.g., OWB ~ 4 μm, single spatial mode) straight waveguide in the back section and angled (4–6°) tapered waveguide section with broad area front waveguide, where the straight waveguide section supports only the fundamental mode. In contrast, a flared laser has a broad area waveguide for both back (e.g., 70–90 μm) and front (e.g., 100 μm) with a slight tapering angle (in this work, $\theta < 0.2o$). The flared laser aims to reduce divergence angle at high output power rather than single-mode operation with lower power of the tapered lasers. The flare angle of the waveguide must be designed properly for the minimal introduction of loss for high efficiency and high-power operation of the LD.

First, we study the effect of various flare designs on the number of TE modes and their divergence angle. Since 975 nm lasers employ compressively strained InGaAs quantum well with TE gain, only these modes are considered. The number of TE modes versus back open window width (OW_B) from 75 μm to 100 μm is calculated for a fixed front open window width (OW_F) of 100 μm as shown in Fig. 4(a). It illustrates that the number of TE modes reduces by one for every ~4 μm (~0.019°) decrease in OW_B for a waveguide with lateral effective index confinement introduced by a ridge waveguide structure ($\Delta n = 0.002$ is implemented in the simulations). Subsequently, the far-field profiles of individual lateral modes are calculated for OW_B of 100 μm (supporting 24 TE modes) and 75 μm (supporting 18 TE modes). Fig. 4(b) shows the angle between two peaks of lateral far-field versus reverse TE mode number (i.e. mode number counted from the highest-order TE mode). The first 15 reverse order modes are calculated as an illustration since the high-order modes contribute dominantly to the high divergence angle of the far-field. The angle between two peaks of lateral far-field declines linearly at a rate of 0.71° and 0.54° per mode for OW_B of 75 μm and 100 μm, respectively, which means a faster reduction of divergence angle for narrower OW_B. The inset demonstrates the far-field profile of a representative mode where the far-field divergence angle is smaller with the narrower back width design for the same reverse mode number. Thus, narrower OW_B designs offer a smaller divergence for high-order modes leading to a reduced far-field divergence angle as a result of the sum of these modes. We consider these results as a guideline for a design of an experiment since the calculation of the overall divergence is a complicated task that should include many other properties such as the weighted contribution of each mode to the divergence, thermal lensing, and nonlinear effects.

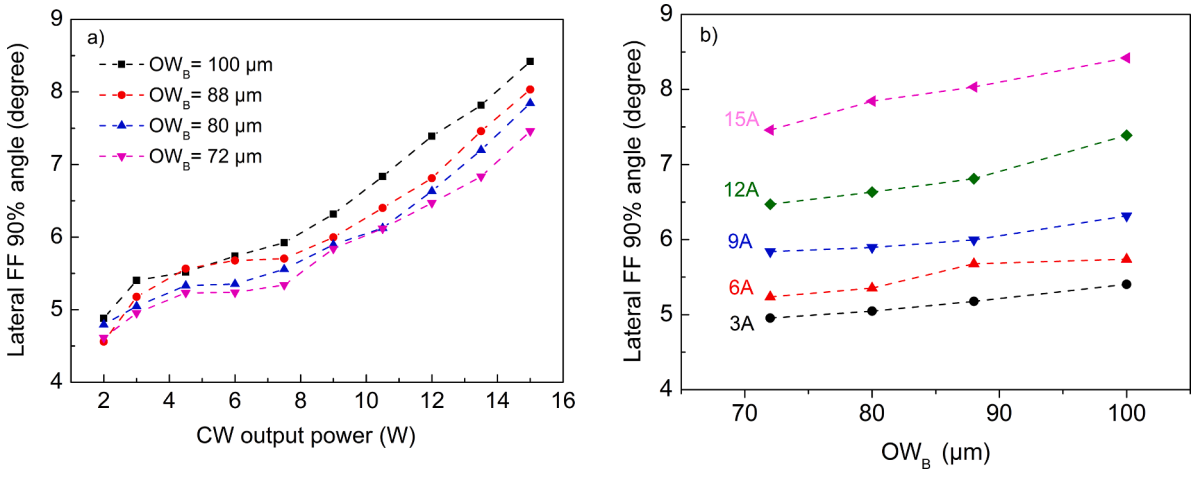

Fig. 5. Experimental results at 25 °C for a) the lateral FF angle versus CW output power for various OW_B, and b) lateral FF angle versus OW_B for various currents.

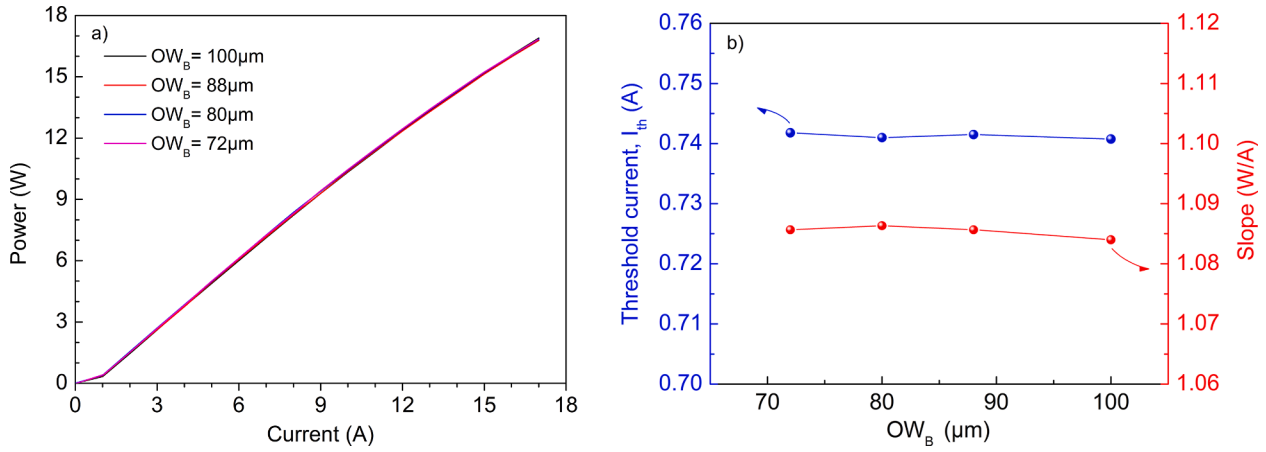

Fig. 6. Experimental results under CW operation at 25 °C for (a) power-current curves of different OW_B, and (b) slope and threshold current versus OW_B.

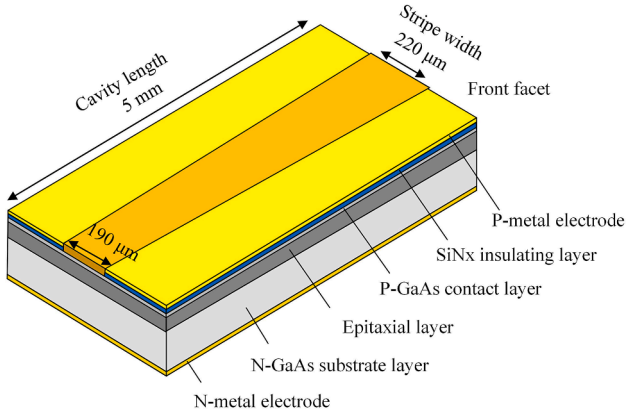

Fig. 7. Simplified illustration of a broad-area laser diode with the flared window structure.

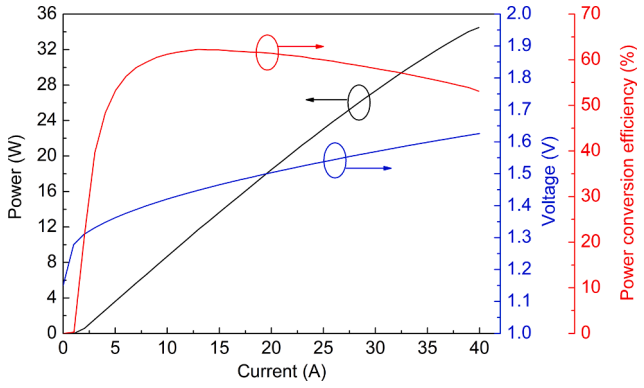

Fig. 8. Power, voltage and efficiency versus current curves at 25 °C under CW operation.

Based on the simulation results, four flared structures were designed with a fixed OW_F of 100 μm and varied OW_B from 72 μm to 100 μm with an angle of 0.178°, 0.127°, 0.076° and 0°, respectively. The experimental results in Fig. 5 (a) show that the lateral far-field divergence angles increase with the CW output power. However, the divergence decreases consistently and significantly for the flared waveguide designs with smaller OW_B sizes. This confirms the expected trend of the simulations in Fig. 4. The lateral far-field angle ($FF_{90\%}$) is as low as 7.4° at 15 W with an OW_B of 72 μm, which is 12% lower than the 100 μm straight design. Fig. 5(b) shows that the effect of lateral divergence angle reduction with the flared design is stronger at higher currents. This is possibly due to the support of more high-order modes with equalized mode gain or better thermal lensing compensation at higher current [26].

The measured L-I data in Fig. 6 (a) show that the output powers have overlapping profiles for the four flared waveguide designs even at the highest tested current of 17 A. The slope efficiency and threshold current are also nearly independent of the OW_B values as shown in Fig. 6 (b). These results confirm that the designs do not introduce optical loss and power penalty on LDs.

4. Scaling laser output to higher power with low divergence angle

The cost of LD chips takes up a large proportion of kW-level laser systems. Hence, there is a strong demand for higher output power per device to reduce the required number of LDs in a system. For this purpose, the dimensions of the LD waveguide have been enlarged over the years to realize higher power operation. To the best of our knowledge, the highest reported CW power from a single emitter LD at room temperature is currently limited to 33 W [23] based on the conventional straight waveguide design. In this section, we present the optimized design details, characterization, and life test results of the LDs demonstrating current-limited output power of 34.5 W and low divergence angle using a flared waveguide design.

The schematic illustration of the 976 nm broad area LD with 0.17° flared open window angle structure is shown in Fig. 7. The layer structure of the epitaxial device was described in section 2 and simulated as in Fig. 1. The epitaxial structure was grown on an n-GaAs substrate by metal-organic vapor phase epitaxy. A Si_3N_4 insulating layer was deposited on the p-contact layer by plasma-enhanced chemical vapor deposition and a window opening is formed for current injection. It is followed by p- and n-metal depositions on the top and bottom contacts, respectively. The cavity length of the single emitter is set as 5 mm. The waveguide is flared with OW_F of 220 μm and OW_B of 190 μm to realize a low lateral divergence angle. The front and rear facets were coated by anti-reflective (~1%) and high-reflective (~98%) films, respectively. The devices were soldered in p-side down configuration with hard solder on high thermal conductivity AlN submounts and bonded on top of Cu heatsinks.

Fig. 8 demonstrates the L-I-V and PCE characteristics of the single emitters under the CW operation at 25 °C. A record-high power of 34.5 W was reached at 40 A (limited by the current source) without catastrophic sudden failure and thermal rollover of the output power. Meanwhile, the PCE was over 53% at 40 A with a low operating voltage of 1.63 V. High PCE of more than 60% was achieved up to 25 W. The slope efficiency, threshold current, operating voltage, and series resistance of the devices were 1.0 W/A, 1.3 A, 1.29 V, 0.006 Ω, respectively.

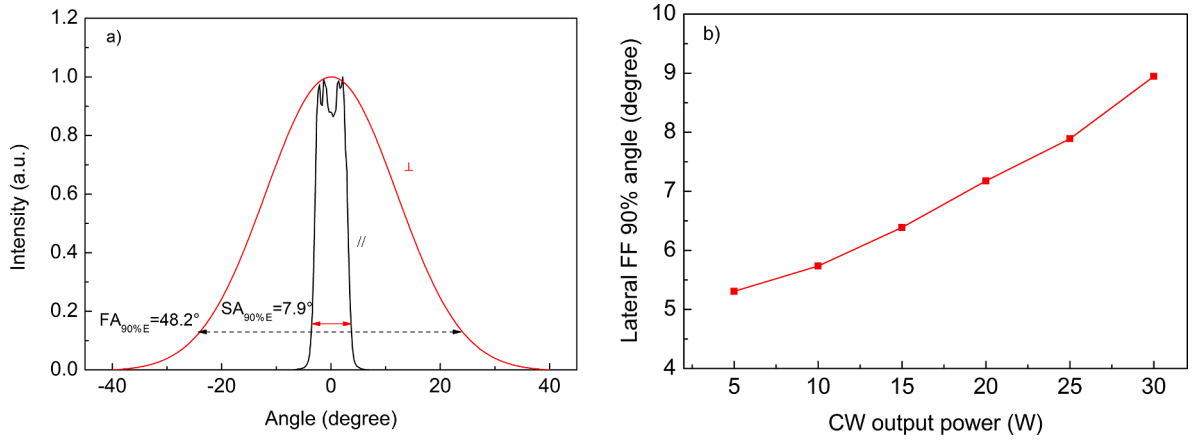

Fig. 9. Experimental results at 25 °C: (a) vertical and lateral divergence angle at 25 W, (b) lateral FF angle vs. CW output power.

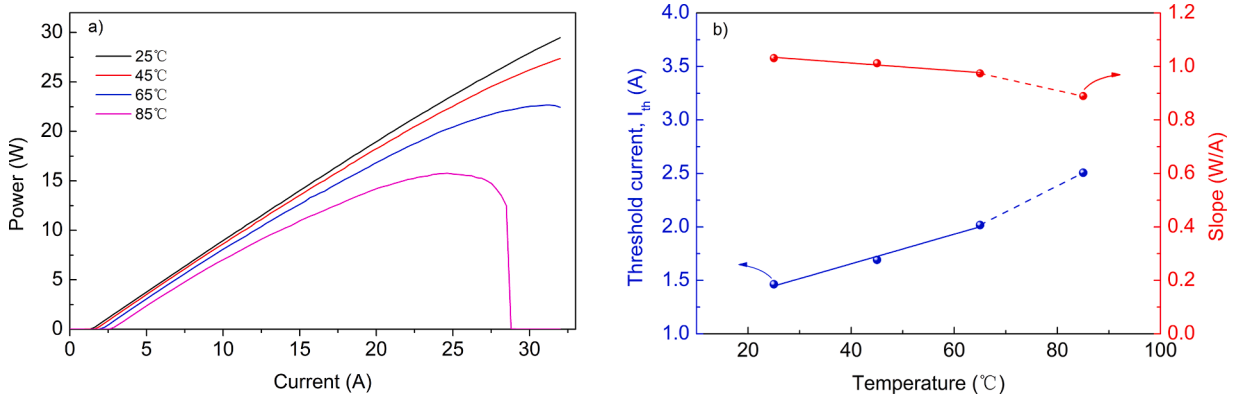

Fig. 10. Temperature sensitivity testing under CW operation: (a) L-I curves at 25 °C, 45 °C, 65 °C, 85 °C, (b) slope and threshold current from 25 °C to 85 °C for T_0 and T_1 (Dots represent the measurement data and lines are the fitting curves).

The thermal resistance is measured as 2.32 K/W based on the linear shift of the lasing wavelength with the dissipated heat load.

Fig. 9a shows the vertical and lateral far-field profiles at an output power of 25 W. The vertical far-field divergence angle with 90% power content is approximately 48.2°, which is in reasonable agreement with the calculated result of 47°. The lateral far-field angle with 90% power content is as low as 7.9°. Fig. 9b illustrates the measured lateral divergence angle as a function of the output power at 25 °C. The lateral divergence angle values are similar to the 100 μm results at relatively low power levels of 5–10 W. However, higher power levels show lower lateral divergence angle most likely due to the lower thermal lensing of larger area compared to that of 100 μm waveguide. The lateral far-field angle is less than 9° even at 30 W, which is beneficial to obtain high brightness at high power.

Fig. 10a shows the L-I curves up to 32 A under CW operation at 25 °C, 45 °C, 65 °C, and 85 °C. Good temperature stability was observed within a range from 25 °C to 65 °C. The maximum output powers at 45 °C and 65 °C maintain high levels, which are more than 27 W and 22.5 W, respectively. Fig. 10b shows the detailed T_0 and T_1 evaluation for the devices. To account for the super-exponential behavior of the characteristic temperatures, we evaluated T_0 and T_1 values separately for 25 °C to 65 °C and 65 °C to 85 °C. The T_0 and T_1 characteristic temperatures are 145 K and 1175 K for 25–65 °C, and 95 K and 487 K for 65–85 °C heatsink temperature.

The LIV and lateral divergence angle results demonstrate the improvement of the proposed designs. Since reliability is critical for high power LDs, life tests were carried to confirm the long-term reliable operation. A total of 39 COSs (chip-on-submounts) have been included in the accelerated lifetime test under a constant injection current of 30 A at a heatsink temperature of 45 °C. The output power is 26.5 W and the junction temperature is estimated as 105 °C. As shown in Fig. 11, 1000 h of accelerated life testing has been completed without any failure. The output power of all the devices has less than 2% variation during the life test demonstrating the high reliability of these devices at high currents.

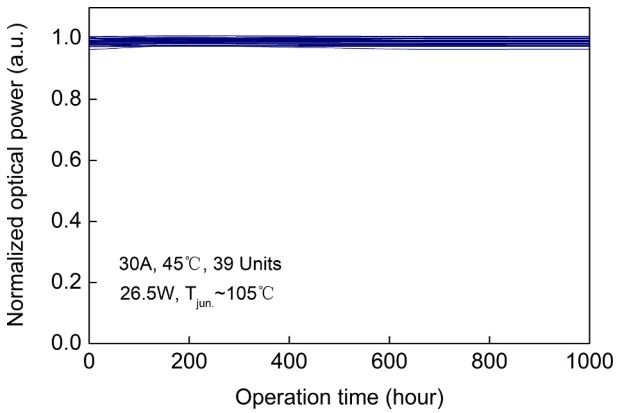

Fig. 11. Accelerated lifetime test for 976 nm broad-area laser diodes.

5. Conclusion

In summary, we presented a flared waveguide design to reduce divergence angle combined with a high-power epitaxial structure at 976 nm. Experimental results show optical absorption loss of 0.47 cm^{-1}, and

high T_0 and T_1 characteristic temperatures of 145 K and 1175 K for 25–65 °C, respectively. Lateral divergence angle behavior was studied and optimized considering the COMD threshold. For an LD with a 5 mm long cavity, 220 μm emitting width, and 0.17° flare angle, the maximum output power is 34.5 W under CW operation at 25 °C. A low lateral far-field divergence angle of less than 8° (90% integrated power) was achieved at 25 W operating output power. To the author's knowledge, this is the highest reported single emitter output power with a low lateral divergence angle for 976 nm LDs. Accelerated life test results demonstrate the reliable operation of these devices showing successful development of the proposed technique for high brightness LDs without additional manufacturing complexity and cost. The results are very encouraging for industrial applications. As a next step, one could employ new designs to achieve a stronger effect on the divergence behavior. The designs and numerical study for reduced divergence can be extended further by combining a flared waveguide with more advanced geometries that might include microstructures [11,27,28,33], spatial filtering techniques [32], and physical mechanisms [24–26]. We believe that a flare design with judicious modification of a waveguide should be used for reduction of the lateral divergence angle for efficient high-power operation of laser diodes.

CRediT authorship contribution statement

Yuxian Liu: Conceptualization, Methodology, Software, Validation, Formal analysis, Investigation, Data curation, Writing - original draft, Writing - review & editing, Visualization. **Guowen Yang:** Conceptualization, Methodology, Formal analysis, Investigation, Resources, Writing - review & editing, Supervision, Project administration, Funding acquisition. **Zhenfu Wang:** Writing - original draft, Writing - review & editing. **Te Li:** Writing - original draft, Writing - review & editing. **Song Tang:** Software, Writing - original draft, Writing - review & editing. **Yuliang Zhao:** Writing - original draft. **Yu Lan:** Writing - review & editing. **Abdullah Demir:** Conceptualization, Methodology, Validation, Formal analysis, Investigation, Writing - original draft, Writing - review & editing, Visualization, Supervision.

Declaration of Competing Interest

The authors declare that they have no known competing financial interests or personal relationships that could have appeared to influence the work reported in this paper.

Acknowledgements

This research did not receive any specific grant from funding agencies in the public, commercial, or not-for-profit sectors.

References

[1] E. Zucker, D. Zou, L. Zavala, H. Yu, P. Yalamanchili, et al., Advancements in laser diode chip and packaging technologies for application in kW-class fiber laser pumping, Proc. SPIE (2014).
[2] K. Yoshikazu, Y. Kyohei, Y. Yuji, N. Ryozaburo, Y. Yumi, et al., Enhanced power conversion efficiency in 900-nm range single emitter broad stripe laser diodes maintaining high power operability, Proc. SPIE (2019).
[3] H. Naito, T. Nagakura, K. Torii, M. Takauji, H. Aoshima, et al., Long-term reliability of 915-nm broad-area laser diodes under 20-W CW operation, IEEE Photonics Technol. Lett. 27 (15) (2015) 1660–1662.
[4] C. Frevert, P. Crump, F. Bugge, S. Knigge, G. Erbert, The impact of low Al-content waveguides on power and efficiency of 9xx nm diode lasers between 200 and 300 K, Semicond. Sci. Technol. 31 (2) (2015) 025003.
[5] H. Yu, et al., 1.2-kW single-mode fiber laser based on 100-W high-brightness pump diodes, Proc. SPIE (2012).
[6] T. Morita, T. Nagakura, K. Torii, M. Takauji, J. Maeda, et al., High-efficient and reliable broad-area laser diodes with a window structure, IEEE J. Sel. Top. Quantum Electron. 19 (2013) 1502104.
[7] I. Petrescu-Prahova, P. Modak, E. Goutain, D. Silan, D. Bambrick, et al., High d/gamma values in diode laser structures for very high power, Proc. SPIE – Int. Soc. Opt. Eng. 7198 (2009).
[8] Y. Yuji, Y. Yumi, M. Masanori, S. Syunta, N. Ryozaburo, et al., 915nm high-power broad area laser diodes with ultra-small optical confinement based on Asymmetric Decoupled Confinement Heterostructure (ADCH), Proc. SPIE (2015).
[9] A. Demir, M. Peters, R. Duesterberg, V. Rossin, E. Zucker, 29.5W continuous wave output from 100um wide laser diode, Proc. SPIE (2015).
[10] A. Demir, M. Peters, R. Duesterberg, V. Rossin, E. Zucker, Semiconductor laser power enhancement by control of gain and power profiles, IEEE Photonics Technol. Lett. 27 (20) (2015) 2178–2181.
[11] L. Wang, C. Tong, S. Shu, F. Sun, Y. Zhao, et al., Loss tailoring of high-power broad-area diode lasers, Opt. Lett. 44 (2019) 3562.
[12] T. Wang, C. Tong, L. Wang, Y. Zeng, S. Tian, et al., Injection-insensitive lateral divergence in broad-area diode lasers achieved by spatial current modulation, Appl. Phys. Express 9 (2016) 112102.
[13] T. Wang, L. Wang, S. Shu, S. Tian, Z. Zhao, et al., Suppression of far-field blooming in high-power broad-area diode lasers by optimizing gain distribution, Chinese Optics Lett. 15 (2017) 071404.
[14] J. Bai, P. Leisher, S. Zhang, S. Elim, M. Grimshaw, et al., Mitigation of thermal lensing effect as a brightness limitation of high-power broad area diode lasers, Proc. SPIE 7953 (2011).
[15] T. Kaul, G. Erbert, A. Maaßdorf, S. Knigge, P. Crump, Suppressed power saturation due to optimized optical confinement in 9xx nm high-power diode lasers that use extreme double asymmetric vertical designs, Semicond. Sci. Technol. 33 (3) (2018) 035005.
[16] J. Piprek, Z.-M. Li, What Causes the Pulse Power Saturation of GaAs-Based Broad-Area Lasers?, IEEE Photonics Technol. Lett. PP (2018) 1-1.
[17] H. Wenzel, P. Crump, A. Pietrzak, X. Wang, G. Erbert, et al., Theoretical and experimental investigations of the limits to the maximum output power of laser diodes, New J. Phys. 12 (8) (2010) 085007.
[18] E.A. Avrutin, B.S. Ryvkin, Effect of spatial hole burning on output characteristics of high power edge emitting semiconductor lasers: a universal analytical estimate and numerical analysis, J. Appl. Phys. 125 (2) (2019) 023108.
[19] E.A. Avrutin, B. Ryvkin, Theory of direct and indirect effect of two-photon absorption on nonlinear optical losses in high power semiconductor lasers, Semicond. Sci. Technol. 32 (2017) 015004.
[20] T. Kaul, G. Erbert, A. Klehr, A. Maabdorf, D. Martin, et al., Impact of carrier non-pinning effect on thermal power saturation in gaas-based high power diode lasers, IEEE J. Selected Topics Quantum Electron. PP (2019) 1-1.
[21] I. Tarasov, N. Pikhtin, S. Slipchenko, Z.N. Sokolova, D. Vinokurov, et al., High power CW (16W) and pulse (145W) laser diodes based on quantum well heterostructures, Spectrochim. Acta Part A Mol. Biomol. Spectrosc. 66 (2007) 819–823.
[22] V. Gapontsev, N. Moshegov, I. Berezin, A. Komissarov, P. Trubenko, et al., Highly-efficient high-power pumps for fiber lasers, 2017.
[23] Y. Kaifuchi, Y. Yamagata, R. Nogawa, R. Morohashi, Y. Yamada, et al., Ultimate high power operation of 9xx-nm single emitter broad stripe laser diodes, 2017.
[24] M. Winterfeldt, P. Crump, H. Wenzel, G. Erbert, G. Trankle, Experimental investigation of factors limiting slow axis beam quality in 9xx nm high power broad area diode lasers, J. Appl. Phys. 116 (2014) 063103.
[25] J. Piprek, S. Li, On the importance of non-thermal far-field blooming in broad-area high-power laser diodes, Appl. Phys. Lett. 102 (2013).
[26] P. Crump, S. Böldicke, C. Schultz, H. Ekhteraei, H. Wenzel, et al., Experimental and theoretical analysis of the dominant lateral waveguiding mechanism in 975 nm high power broad area diode lasers, Semicond. Sci. Technol. 27 (2012) 045001.
[27] M. Miah, S. Strohmaier, G. Urban, D. Bimberg, Beam quality improvement of high-power semiconductor lasers using laterally inhomogeneous waveguides, Appl. Phys. Lett. 113 (2018) 221107.
[28] J. Rong, E. Xing, L. Wang, S. Shu, S. Tian, et al., Control of lateral divergence in high-power, broad-area photonic crystal lasers, Appl. Phys Express 9 (2016) 072104.
[29] E.S. Kintzer, J.N. Walpole, S.R. Chinn, C.A. Wang, L.J. Missaggia, High-power, strained-layer amplifiers and lasers with tapered gain regions, IEEE Photonics Technol. Lett. 5 (6) (1993) 605–608.
[30] P. Adamiec, B. Sumpf, I. Rüdiger, J. Fricke, K.-H. Hasler, et al., Tapered lasers emitting at 650 nm with 1 W output power with nearly diffraction-limited beam quality, Opt. Lett. 34 (16) (2009) 2456–2458.
[31] H. Odriozola, J.M.G. Tijero, L. Borruel, I. Esquivias, H. Wenzel, et al., Beam properties of 980-nm tapered lasers with separate contacts: experiments and simulations, IEEE J. Quantum Electron. 45 (1) (2009) 42–50.
[32] S. Gawali, D. Gailevičius, G. Garre-Werner, V. Purlys, C. Cojocaru, et al., Photonic crystal spatial filtering in broad aperture diode laser, Appl. Phys. Lett. 115 (14) (2019) 141104.
[33] M. Radziunas, M. Botey, R. Herrero, K. Staliunas, Intrinsic beam shaping mechanism in spatially modulated broad area semiconductor amplifiers, Appl. Phys. Lett. 103 (2013) 132101.
[34] H.-C. Eckstein, U. Zeitner, A. Tünnermann, W. Schmid, U. Strauss, et al., Mode shaping in semiconductor broad area lasers by monolithically integrated phase structures, Opt. Lett. 38 (2013) 4480–4482.
[35] Z. Wang, T. Li, G. Yang, Y. Song, High power, high efficiency continuous-wave 808 nm laser diode arrays, Opt. Laser Technol. 97 (2017) 297–301.
[36] S. Slipchenko, D. Vinokurov, N.A. Pikhtin, Z.N. Sokolova, A. Stankevich, et al., Ultralow internal optical loss in separate-confinement quantum-well laser heterostructures, Semiconductors 38 (2004) 1430–1439.
[37] K. Hasler, H. Wenzel, P. Crump, S. Knigge, A. Maasdorf, et al., Comparative theoretical and experimental studies of two designs of high-power diode lasers, Semicond. Sci. Technol. 29 (2014) 045010.